Phase diagram of $Ti_{50-x}Ni_{50+x}$: Crossover from martensite to strain glass

Zhen Zhang,[1,2] Yu Wang,[2] Dong Wang,[1] Yumei Zhou,[1,2] Kazuhiro Otsuka,[2] and Xiaobing Ren[1,2,*]
[1]*Multi-Disciplinary Materials Research Center and State Key Laboratory for Mechanical Behavior of Materials, Frontier Institute of Science and Technology, Xi'an Jiaotong University, Xi'an 710049, People's Republic of China*
[2]*Ferroic Physics Group, National Institute for Materials Science, Tsukuba, 305-0047 Ibaraki, Japan*
(Received 2 February 2010; revised manuscript received 7 April 2010; published 2 June 2010)

We systematically investigated the variation in transition behavior and physical properties over a wide excess Ni (acting as defect) concentration range ($x=0-2.5$) in $Ti_{50-x}Ni_{50+x}$ alloys. This enables the establishment of an updated quantitative phase diagram for this important system. The phase diagram shows not only the well-known parent phase and martensite phase but also a premartensitic state and a strain glass state. Our experiments were able to determine quantitatively the borders of these states, the latter two having been unclear so far. The new phase diagram shows that a crossover from martensite to strain glass occurs at $x=1.3$, and the appearance of a "premartensitic phase" below a critical temperature T_{nd} for defect-containing compositions ($x>0$). We propose that point defects (excess Ni here) play two roles in a ferroelastic/martensitic system: (i) changing the thermodynamic driving force for the formation of long-range strain order (martensite) and (ii) creating random local stress that favors a premartensitic nanostructure and strain glass. Our work enables a simple explanation for several long-standing puzzles, such as the appearance of premartensitic nanostructure, the vanishing of transition latent heat with increasing Ni content and the anomalous negative temperature coefficient of electrical resistivity in Ni-rich Ti-Ni alloys.

DOI: 10.1103/PhysRevB.81.224102 PACS number(s): 64.70.K−, 64.70.P−, 61.43.Fs, 81.30.Kf

I. INTRODUCTION

Shape memory alloys are important functional materials owing to their shape memory effect and superelastic behavior.[1] These important properties originate from a spontaneous lattice-distorting transition called martensitic transition. Among many shape memory alloys, Ti-Ni alloy is the most important one for its good shape memory properties in combination with superior mechanical properties.[2] In practice, Ti-Ni alloy is often doped with excess Ni or a third element (such as Fe, Cu, etc.) to further modify its shape memory effect and superelastic behavior. Thus understanding the effect of doping (which can be viewed as point defects) on the transition behavior of Ti-Ni alloy is of significant practical and fundamental importance and has been subject to intensive investigations.[2]

The undoped or stoichiometric $Ti_{50}Ni_{50}$ undergoes a B2-B19′ martensitic transition at 333 K. With doping excess Ni (self-doping) to Ti-Ni alloy, the transition behavior of Ni excess $Ti_{50-x}Ni_{50+x}$ shows interesting changes. At low Ni doping level ($x<1$), the B2-B19′ martensitic transition by itself remains unchanged; but the martensitic transition temperature M_s and the corresponding transition latent heat show a drastic decrease.[3] It remains unclear for decades why excess-Ni doping can cause a vanishing transition latent heat. Moreover, excess Ni causes another well observed but puzzling phenomenon, i.e., a defect-induced precursor state with premartensitic nanostructure appears above M_s,[4,5] such nanostructure being unexpected for an ideal parent phase.[6,7] The appearance of defect-induced precursor state (in the form of either nanocluster or tweed pattern) is quite common in many martensitic systems such as Ti-Ni-Fe,[8] Ni-Al,[9,10] and Co-Ni-Ga.[11] Furthermore, the precursor state of Ni-rich Ti-Ni martensitic alloy seems to exhibit an anomalous negative temperature coefficient of electrical resistivity,[12] being opposite to the metallic nature of this alloy;[13] this has remained a puzzle for a long time.

At high Ni doping level ($x>1.5$), previous differential scanning calorimetry (DSC) and resistivity measurement indicated that the B2-B19′ martensitic transition vanishes.[14] Such a "nontransforming" behavior at high doping level sharply contrasts with the martensitic transition behavior at low-doping level. However, recent studies have shown that the high Ni-doped $Ti_{50-x}Ni_{50+x}$ alloy is not nontransforming; it actually undergoes a new type of transition called strain glass (STG) transition.[15] The STG is a frozen strain-disordered state analogous to the window glass, a frozen structurally disordered state.[16,17] Moreover, strain glass is not a unique property of Ti-Ni system only; it has also been found in quite an increasing number of other systems.[18,19] It is likely to be a general phenomenon in ferroelastic systems with sufficient amount of point defects.[20] The STG transition can be detected experimentally by observing the following glass signatures:[21] (1) frequency-dependent anomaly of ac mechanical susceptibility obeying Vogel-Fulcher relation,[15,22,23] (2) nonergodicity as revealed in the zero field cooling (ZFC)/ field cooling (FC) experiment,[24] and (3) no change in average structure.[15,25]

It should be noted that similar glassy phenomenon has been discovered in other ferroic systems, e.g., ferroelectric relaxor, where electrical polarization undergoes a freezing transition. In relaxor systems the glass signatures are almost identical to those of strain glass, such as the Vogel-Fulcher relation in ac dielectric susceptibility,[26] frequency-dependent mechanical susceptibility,[27] and nonergodicity shown in the ZFC/FC curves.[28] Therefore, glassy phenomenon is a quite general phenomenon in different classes of ferroic systems.[20]

A preliminary and schematic phase diagram of $Ti_{50-x}Ni_{50+x}$ showing a strain glass has been suggested by our recent study.[15] Based on this phase diagram, a generic phase diagram of ferroelastic system as a function of point-defect

concentration has been proposed recently.[20] In the phase diagram, it has been shown that point defects induce a "precursory nanostructure state" prior to the formation of normal martensite state and of strain glass state. However, a quantitative phase diagram and a systematic study of this first strain glass system are still lacking. In particular the following important issues closely related to point defects remain unclear: (1) the role of point defect (excess Ni here) in the crossover from martensite to strain glass, (2) the nature and the temperature/composition range of the premartensitic tweed or nanostructure, (3) the origin of the vanishing latent heat with increasing Ni content, and (4) the origin of negative temperature coefficient of electrical resistivity in Ni-rich Ti-Ni alloy. The determination of a quantitative crossover phase diagram and the clarification of the above key questions will significantly progress our understanding on this important system.

In present study, we systematically investigated the variation in transition behavior and physical properties of $Ti_{50-x}Ni_{50+x}$ binary system from pure martensite ($x=0$) to highly doped strain glass ($x=2.5$). This leads to the establishment of a quantitative phase diagram for $Ti_{50-x}Ni_{50+x}$ binary system over a wide temperature and composition range. This phase diagram reveals the evolution of all the states (parent phase, martensite, precursory nanostructure state, and strain glass state) in the system as a function of temperature and defect concentration. Our study suggests a twofold effect of point defects: (i) changing thermodynamic driving force to form long-range strain order (i.e., martensite), (ii) creating random local stress field that favors local strain order. This new insight enables a microscopic explanation not only for the nature of all the phases (including the precursor and strain glass) appearing in the new phase diagram but also for several long-standing puzzles, such as the vanishing transition latent heat with increasing Ni doping and the anomalous negative temperature coefficient of electrical resistivity of Ni-rich Ti-Ni alloy.

II. EXPERIMENT

$Ti_{50-x}Ni_{50+x}$ alloys with excess Ni concentration $x=0$, 1, 1.3, 1.5, and 2.5 were studied by various techniques. The $x=0$, 1, 1.3, and 1.5 samples were supplied by Furukawa Electric Co. Ltd. The $x=2.5$ sample was made by induction melting in Ar atmosphere. To obtain a homogeneous supersaturated Ni-rich Ti-Ni solid solution, all the samples were sealed in evacuated quartz tubes and annealed at 1273 K for 1 h, then followed by water quenching.

The variation in the transition behavior as a function of defect concentration (x) in $Ti_{50-x}Ni_{50+x}$ samples was monitored by three sets of measurements: DSC, electrical resistivity, and dynamic mechanical analysis (DMA). These measurements can also determine the boundaries among all the possible states in $Ti_{50-x}Ni_{50+x}$ alloys, which include (i) parent phase (dynamically disordered strain state), (ii) martensitic state (long-range ordered strain state), (iii) precursory nanostructure state (quasidynamically disordered strain state, as will be discussed later), which is usually called precursor state in martensitic composition regime and unfrozen strain glass in the strain glass composition regime,[29] and (iv) frozen strain glass (frozen disordered strain state).

To characterize the transition latent heat of $Ti_{50-x}Ni_{50+x}$ samples, differential scanning calorimetry measurement was performed in DSC Q200 of TA Instruments with a heating/cooling rate of 10 K/min. This measurement can reveal the martensitic transition and determine the phase boundary between parent phase and martensite phase or between precursor state and martensite phase.

Electrical-resistivity measurement is a sensitive probe for the onset of martensitic transition. It is also very sensitive to the slight change in the local structure prior to the martensitic transition, i.e., the appearance of premartensitic nanostructure.[30] Thus, we applied electrical-resistivity measurement to determine the onset of static local strain order (i.e., the precursor state and the unfrozen strain glass) from the ideal parent phase (without static local strain order), as well as the onset of martensitic transition. Electrical-resistivity measurement was performed with a four-terminal method at a constant current of 100 mA. The sample temperature was measured by a thermocouple spot welded onto the sample. The temperature ramp was done in a temperature chamber at a heating/cooling rate of 2 K/min. With this measurement, the phase boundary between parent phase and precursor state and that between parent phase and unfrozen strain glass were determined (an analysis of the relation between resistivity and the onset of precursor state is given in Sec. V).

Dynamic mechanical analysis was used not only to identify a transition but also to determine if it is a normal martensitic transition (without frequency dispersion) or a strain glass transition (with frequency dispersion and obeying Vogel-Fulcher relation).[15,22,23] A DMA Q800 from TA Instruments was used for this measurement. The ac storage modulus and internal friction were tested in the frequency range of 0.2–20 Hz with an ac displacement amplitude of 20 μm in the single cantilever mode. To ensure the temperature homogeneity and the accuracy of temperature, the specimen was held for 5 min at each temperature before recording the DMA data. With the DMA measurement, the phase boundary between parent phase (or precursor state) and martensite, and that between unfrozen strain glass and frozen strain glass can be determined.

III. RESULTS

In this part, we will show the DSC, electrical resistivity, and DMA results of $Ti_{50-x}Ni_{50+x}$ alloys as a function of excess Ni concentration x ($0 \le x \le 2.5$); this reveals clearly how point defects (excess Ni here) change the transition behavior of this system. Moreover, these results also determined quantitatively the martensitic transition temperature M_s, the onset temperature T_{nd} ("nd" stands for "nanodomain") of the precursor state (or unfrozen strain glass), and the ideal freezing temperature T_0 for strain glass transition; thereby the phase boundaries of this system can be determined.

A. Phase transition behavior of pure martensitic $Ti_{50}Ni_{50}$ ($x=0$)

The transition properties of pure $Ti_{50}Ni_{50}$ martensitic alloy are shown in Figs. 1(a)–1(d). The $B2 \rightarrow B19'$ martensitic

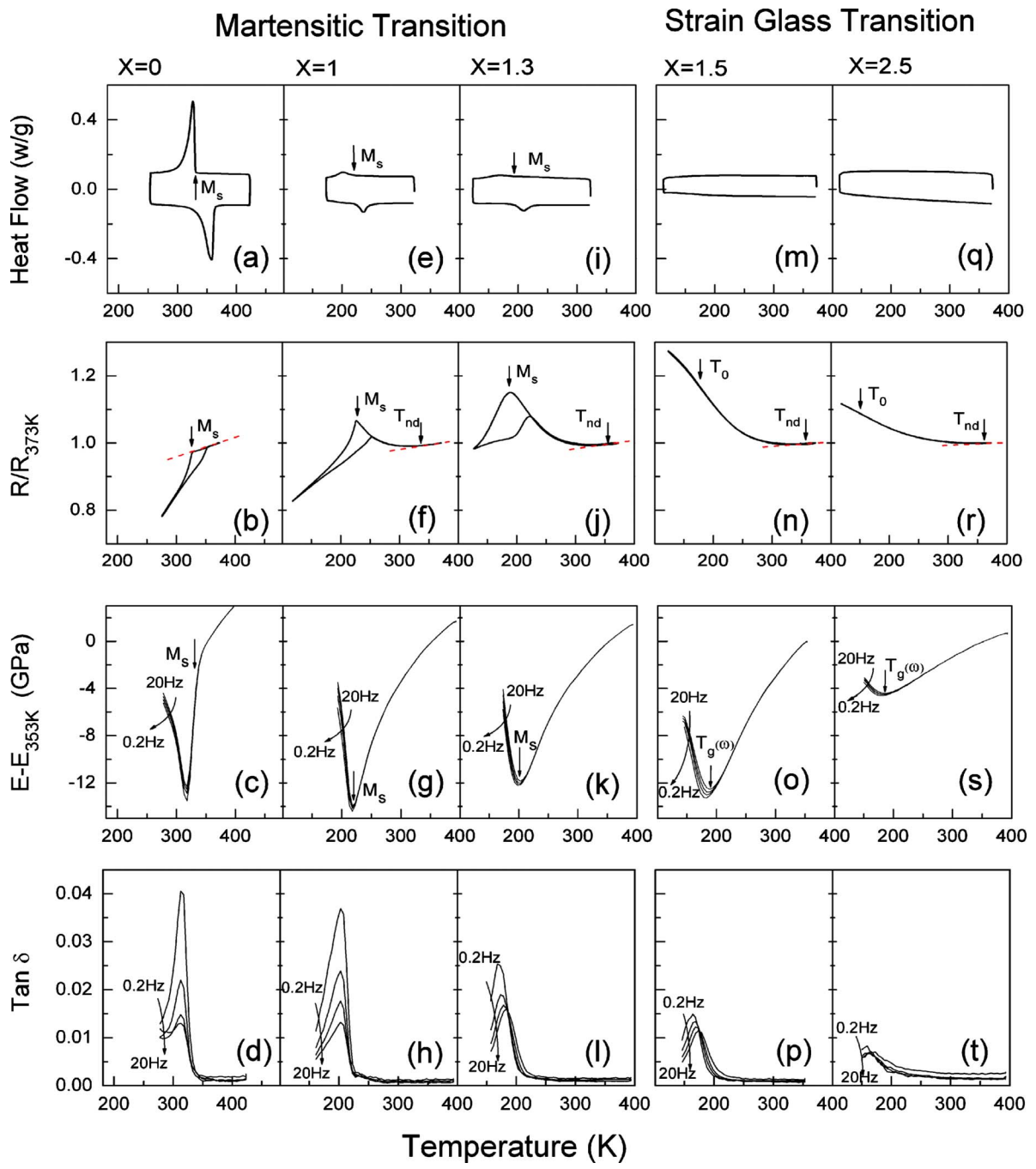

FIG. 1. (Color online) Transition behavior of $Ti_{50-x}Ni_{50+x}$ alloys as function of excess Ni (point-defect) concentration $x(=0-2.5)$. (a), (e), (i), (m), and (q) show the heat flow; (b), (f), (j), (n), and (r) show the normalized electrical resistivity $R/R_{373\ K}$; (c), (g), (k), (o), and (s) show the normalized storage modulus $E-E_{353\ K}$; (d), (h), (l), (p), and (t) show the internal friction tan δ. M_s is the start temperature of martensitic transition; $T_g(\omega)$ is the freezing temperature at different frequency ω (0.2–20 Hz); T_0 is the ideal freezing temperature of strain glass; T_{nd} is the onset temperature of precursor state and unfrozen strain glass which is defined by the onset of the deviation from the linear resistivity decrease as shown in the figures.

transition at its transition temperature M_s is accompanied by a latent heat peak in the DSC curve [Fig. 1(a)]. It is also characterized by a sharp decrease in electrical resistivity [Fig. 1(b)]. In this defect-free (excess-Ni-free) stoichiometric sample, there is no anomaly in the electrical resistivity prior to the onset temperature of martensitic transition (M_s) and the resistivity decreases linearly above M_s [Fig. 1(b)]. This is a key feature of the parent phase with dynamically disordered strain and is to be compared with the resistivity behavior of defect-containing compositions ($x>0$) to be shown in the following. The martensitic transition is also reflected in the ac mechanical properties of $Ti_{50}Ni_{50}$, which is characterized by a frequency-independent dip in storage modulus [Fig. 1(c)] and a frequency-independent peak in internal friction [Fig. 1(d)]. The frequency independence in the DMA dip/peak is an important feature of martensitic transition.

B. Phase transition behavior of $Ti_{50-x}Ni_{50+x}$ at low-defect concentration ($0 < x \leq 1.3$)

The transition behavior of $Ti_{50-x}Ni_{50+x}$ alloys at low-defect content ($x=1$ and 1.3) is shown in Figs. 1(e)–1(l). As will be detailed below, all these results demonstrate that the $Ti_{50-x}Ni_{50+x}$ ($x=1$ and 1.3) alloys exhibit martensitic transition, but the martensitic transition in these defect-containing alloys is dramatically modified with increasing point-defect concentration, compared with that of pure $Ti_{50}Ni_{50}$ alloy.

The existence of martensitic transition in $Ti_{50-x}Ni_{50+x}$ ($x=1$ and 1.3) alloys is indicated in Figs. 1(e)–1(l). This is revealed by the latent-heat peak in the DSC curves [Figs. 1(e) and 1(i)], and the sharp drop of electrical resistivity [Figs. 1(f) and 1(j)] in these alloys. In addition, DMA measurement shows a frequency-independent dip in storage modulus [Figs. 1(g) and 1(k)] and a frequency-independent peak in internal friction [Figs. 1(h) and 1(l)] for $Ti_{50-x}Ni_{50+x}$ ($x=1$ and 1.3); such a feature is the same as that of pure $Ti_{50}Ni_{50}$ martensitic alloy.

Although the above results show that the $Ti_{50-x}Ni_{50+x}$ ($x=1$ and 1.3) alloys with low-defect content undergo normal martensitic transition like the defect-free $Ti_{50}Ni_{50}$, their transition features are greatly changed by point defects (excess Ni here). As shown in Figs. 1(a)–1(l), the DSC curves, electrical-resistivity curves, and dynamic mechanical properties show that the martensitic transition temperature M_s decreases sharply as Ni concentration increases from $x=0$ to 1.3. In addition, Figs. 1(a)–1(l) demonstrate that the martensitic transition of $Ti_{50-x}Ni_{50+x}$ alloys becomes gradually smeared with increasing doping level x. As seen in Figs. 1(e) and 1(i), the latent-heat peak of $Ti_{50-x}Ni_{50+x}$ ($x=1$ and 1.3) alloys becomes broader with increasing x. Similar broadening of martensitic transition caused by point defects is also reflected in electrical-resistivity [Figs. 1(f) and 1(j)] and ac mechanical properties [Figs. 1(g), 1(h), 1(k), and 1(l)]. In the meantime, the magnitude of DSC peak [Figs. 1(e) and 1(i)] and the storage modulus dip become less prominent [Figs. 1(g) and 1(k)] and the loss peak becomes smaller [Figs. 1(h) and 1(l)] with increasing x, which demonstrate the signature of martensitic transition in $Ti_{50-x}Ni_{50+x}$ ($x=1$ and 1.3) alloys is weakened by point defects.

The point defects not only modify the feature of martensitic transition as shown above but also cause a precursor state with nanosized domains above M_s, which has been well observed in Ti-Ni (Ref. 4) and Ti-Ni-Fe (Ref. 30) martensitic alloys. As will be discussed in Sec. V, the onset of the deviation from linearity in the electrical-resistivity vs temperature curve above M_s shown in Figs. 1(f) and 1(j) can be defined as the onset temperature T_{nd} of the precursor state for $Ti_{50-x}Ni_{50+x}$ ($x=1$ and 1.3) martensitic alloys. The T_{nd} in martensitic system is physically similar to the Burns temperature[31,32] in defects-doped ferroelectric system, which is defined as the onset temperature of quasistatic nanopolar domains prior to its ferroelectric transition. The system is in a normal parent phase with dynamically disordered strain at $T > T_{nd}$, but shows a crossover into the precursor state due to the appearance of small amount of quasistatic nanodomains at $T < T_{nd}$ and the formation of these nanodomains causes the increase in the resistivity of $Ti_{50-x}Ni_{50+x}$ ($x=1$ and 1.3) alloys.

C. Phase-transition behavior of $Ti_{50-x}Ni_{50+x}$ with high-defect concentration ($x \geq 1.5$)

The properties of $Ti_{50-x}Ni_{50+x}$ alloys with high-defect content ($x=1.5$ and 2.5) are shown in Figs. 1(m)–1(t), which demonstrate that the martensitic transition signatures vanish but the strain glass transition features appear instead. As shown in Figs. 1(m) and 1(q), the DSC curves for $Ti_{50-x}Ni_{50+x}$ ($x=1.5$ and 2.5) alloys do not exhibit detectable latent-heat peak, which means the transition entropy equals to zero. This demonstrates the martensitic transition disappears at high-defect concentration regime. The vanishing martensitic transition in these two alloys can also be seen from the electrical resistivity. As shown in Figs. 1(n) and 1(r), the electrical resistivity for $Ti_{50-x}Ni_{50+x}$ ($x=1.5$ and 2.5) alloys keep on increasing with decreasing temperature, which sharply contrasts with the drop of electrical resistivity during the B2-B19′ martensitic transition in $Ti_{50-x}Ni_{50+x}$ ($x=0$, 1, and 1.3) alloys. It should be mentioned that the disappearance of martensitic transition in Ni-rich Ti-Ni alloy has been confirmed previously by similar DSC and electrical-resistivity measurement.[14] Our results are consistent with the previous results.

The DSC and electrical-resistivity results show that $Ti_{50-x}Ni_{50+x}$ ($x=1.5$ and 2.5) alloys with high-defect content do not undergo martensitic transition. However, their dynamic mechanical properties show anomalies, which indicates that the system actually undergoes a transition being different from the martensitic transition. As shown in Figs. 1(o), 1(p), 1(s), and 1(t), the $Ti_{50-x}Ni_{50+x}$ ($x=1.5$ and 2.5) alloys exhibit a broader storage modulus dip and a smaller internal friction peak than those [Figs. 1(c), 1(d), 1(g), 1(h), 1(k), and 1(l)] in lightly doped martensitic $Ti_{50-x}Ni_{50+x}$ alloys ($x < 1.3$). More importantly, the storage modulus dip temperature and internal-friction peak temperature of $Ti_{50-x}Ni_{50+x}$ ($x=1.5$ and 2.5) alloys shift with different frequencies, which is fundamentally different from the frequency-independent behavior of $Ti_{50-x}Ni_{50+x}$ ($x \leq 1.3$) martensitic alloys. The frequency dispersion of storage modulus of $Ti_{50-x}Ni_{50+x}$ ($x=1.5$ and 2.5) alloys follows the Vogel-Fulcher relation, as exemplified by the dip temperature vs frequency of $Ti_{48.5}Ni_{51.5}$ strain glass in Fig. 2, which demonstrates a dynamic freezing transition—strain glass transition occurs in highly doped alloys. The ideal freezing temperature T_0 of $Ti_{50-x}Ni_{50+x}$ ($x=1.5$ and 2.5) strain glass can be obtained by fitting the storage modulus dip temperature vs frequency data with Vogel-Fulcher relation. Very interestingly, the resistivity curves of these two strain glass alloys show an inflection point at their ideal freezing temperatures T_0, which are indicated in Figs. 1(n) and 1(r). These results demonstrate that the freezing transition of strain glass can also be identified by a simple electrical-resistivity measurement.

Above the strain glass transition, the strain glass alloys stay in their unfrozen state, in which quasistatic martensitic nanodomains are also observed.[20] The change from parent phase to unfrozen strain glass can also be reflected from electrical resistivity. As shown in Figs. 1(n) and 1(r), the electrical resistivity of $Ti_{50-x}Ni_{50+x}$ ($x=1.5$ and 2.5) strain glass alloys shows a deviation from linearity below T_{nd}

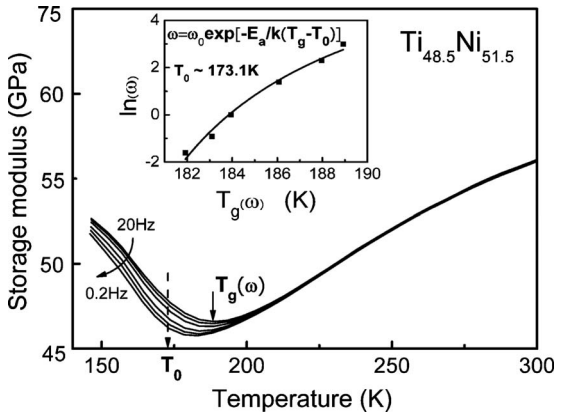

FIG. 2. Temperature dependence of storage modulus of $Ti_{50-x}Ni_{50+x}$ ($x=1.5$) strain glass at various frequencies (0.2–20 Hz). The inset shows that the relation between freezing temperature $T_g(\omega)$ and $\ln(\omega)$ can be fitted well by the Vogel-Fulcher relation and ideal freezing temperature T_0 is determined to be 173.1 K.

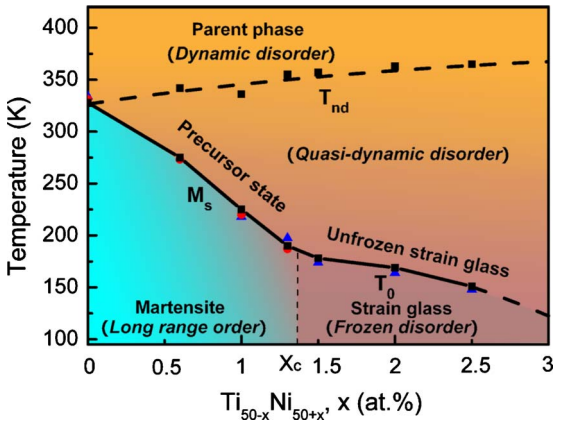

FIG. 3. (Color online) Temperature-composition phase diagram of $Ti_{50-x}Ni_{50+x}$ binary system. The onset temperature T_{nd} of precursor state and unfrozen strain glass is determined by electrical-resistivity measurement. The martensitic transition temperature M_s is determined by DSC, DMA, and electrical-resistivity measurement. The ideal freezing temperature of strain glass T_0 is determined by DMA and electrical-resistivity measurement (inflection point of the resistivity curve, explained in Sec. III C). Here, ▲ represents DMA results; ● represents DSC results; and ■ represents electrical-resistivity results.

above their T_0. It corresponds to the onset temperature of the unfrozen strain glass, which will be discussed in Sec. V. It should be noted that both the precursor state of $Ti_{50-x}Ni_{50+x}$ ($x=1$ and 1.3) martensitic alloys and unfrozen strain glass state of $Ti_{50-x}Ni_{50+x}$ ($x=1.5$ and 2.5) strain glass alloys show similar abnormal increase in electrical resistivity below T_{nd}. It is because the intrinsic nature of precursor state in martensitic composition regime and unfrozen strain glass state in strain glass composition regime is the same,[29] and this point will be further discussed later.

IV. PHASE DIAGRAM OF $TI_{50-x}NI_{50+x}$—CROSSOVER FROM MARTENSITE TO STRAIN GLASS AND THE EXISTENCE OF A PRECURSOR STATE

The above systematic experimental results demonstrate how the transition features gradually change as a function of defect concentration (excess Ni here). They also enable us to determine M_s, T_{nd}, and T_0 as a function of defect concentration x, which are the borders-separating parent phase, martensite, precursor state, and unfrozen and frozen strain glass state, respectively. Therefore, a quantitative phase diagram of $Ti_{50-x}Ni_{50+x}$ can be established. Such a phase diagram will reveal a key phenomenon: point defects cause the crossover from martensite to strain glass.

The phase diagram of $Ti_{50-x}Ni_{50+x}$ is shown in Fig. 3. All the $Ti_{50-x}Ni_{50+x}$ compositions are in the parent phase state at very high temperature, being independent of defect concentration, however, the phase transition follows very different paths and results in very different products with increasing defect concentration x. At $x=0$, i.e., pure $Ti_{50}Ni_{50}$, the system transforms directly into B19′ martensite at its M_s. However, with doping small amount of excess Ni ($x<x_c$), the parent phase cannot transform into martensite directly, instead it first changes into a precursor state at T_{nd} on cooling and then the precursor state transforms into the martensite at M_s on further cooling. The precursor state is characterized by the onset of the deviation from linearity in the electrical-resistivity vs temperature curve [Figs. 1(f), 1(j), 1(n), and 1(r)], and this will be discussed in detail in the discussion part. When $x>x_c$ (~ 1.3), the high-temperature parent phase first changes to the unfrozen strain glass at T_{nd} on cooling, which is a similar state as the precursor state of $x<x_c$ and is characterized by a similar anomaly in resistivity. But this unfrozen strain glass state does not transform into normal martensite upon cooling; instead it transforms into a frozen strain glass state at its ideal freezing temperature T_0. Notably, the phase diagram indicated that the precursor state and unfrozen strain glass state are of the same physical nature, differing only in defect concentration x. As will be discussed in more detail later, both states represent a quasidynamically disordered strain state, as evidenced by recent experimental study[29] and can also been seen from the similar electrical-resistivity vs temperature behavior in present study.

The new Ti-Ni phase diagram in Fig. 3 provides important clues for understanding why point defects can cause a crossover from martensite to strain glass. The lowering of the martensitic transition temperature M_s with increasing point-defect concentration x is the first effect of excess Ni. It indicates that point defects significantly lower the thermodynamic stability of the martensitic state, i.e., making long-range strain-ordering (=martensite) temperature decrease drastically. However, this effect alone cannot explain why the system has to go to strain glass at high-defect concentration. The appearance of strain glass (i.e., frozen local strain order) at $x>x_c$ can be explained only if we consider that point defects introduce random local stresses. Such local stress fields dedicate local strain ordering, and thus produce randomly distributed nanodomains,[6,7] as will be shown in Sec. V. Thus excess Ni (as point defect) favors local strain order and suppresses the formation of long-range strain ordering (i.e., martensite). As the result, at low temperature the nanodomains are frozen due to a kinetic reason and this is

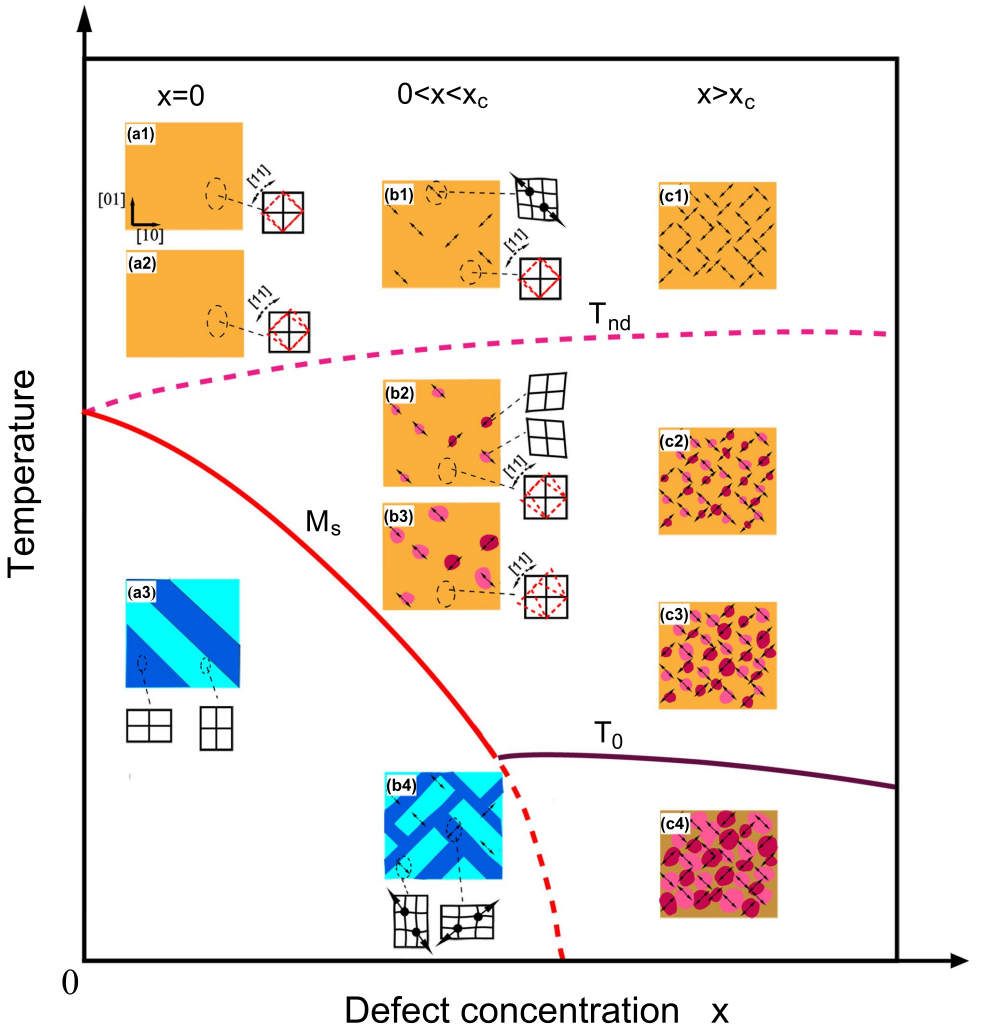

FIG. 4. (Color online) Microscopic picture about the crossover behavior from normal martensitic transition to strain glass transition as a function of defect concentration. The lowering thermal dynamic driving force by doping point defects is represented by the sharp decrease in M_s with increasing x. The point-defects-induced random stress fields are expressed by ↔. (a1), (a2), and (a3) show the transition process of pure martensitic system from dynamically disordered state [(a1) and (a2)] to long-range ordered state (a3). (b1), (b2), (b3), and (b4) show the transition process of slightly doped martensitic system from dynamically disordered state (b1) to quasidynamically disordered state [(b2) and (b3)], finally to long-range ordered state (b4). (c1), (c2), (c3), and (c4) show the freezing process of strain glass system (with high-defect concentration) from a dynamically disordered state (c1) to quasidynamically disordered state [(c2) and (c3)], finally to frozen disordered state (c4).

the observed strain glass transition. In the discussion part we shall reveal in detail how point defects result in the crossover behavior from martensite to strain glass.

V. DISCUSSION

In the following, we propose a simple and generic physical picture about why and how the point defect can induce the crossover from normal martensitic transition into strain glass transition, as shown in Fig. 3. It also describes the physical nature of all the states in the phase diagram (Fig. 3) and provides a simple explanation to several long-standing puzzles, such as the vanishing transition entropy with increasing Ni doping and the anomalous negative temperature coefficient of resistivity in Ni-rich Ti-Ni alloys.

A. Physical nature of defect-containing ferroelastic/martensitic systems: The dual role of point defects

1. Defect-free system (i.e., x=0): Dynamic disorder→long-range order

The physical picture for the martensitic transition in a defect-free martensitic system is shown in Figs. 4(a1), 4(a2), and 4(a3). At the temperature above M_s, the system is in the parent phase state, which is a dynamically disordered strain state with heterophase fluctuation, i.e., instantaneous low-symmetry clusters [Fig. 4(a1)],[33] but the average crystal symmetry remains cubic. This is analogous to the similar physical picture of the paramagnetic state[34] and paraelectric state.[35] The magnitude of the heterophase fluctuation in parent phase increases with lowering temperature [Fig. 4(a2)],[36]

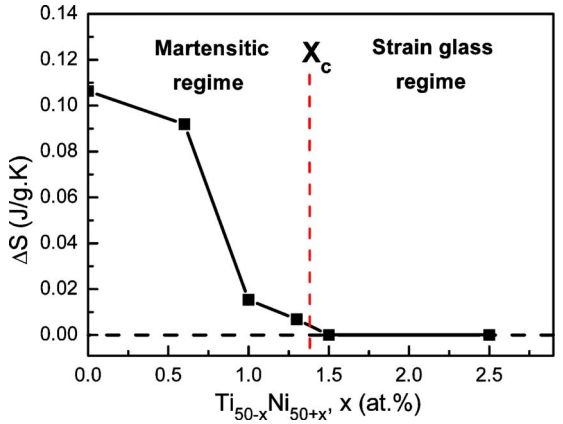

FIG. 5. (Color online) The transition entropy ΔS as a function of defect concentration x in $Ti_{50-x}Ni_{50+x}$ alloys.

until forming a static long-range strain order (=martensite) at M_s [Fig. 4(a3)].[37,38]

2. *Low-defect concentration* ($0<x<x_c$)*: Dynamic disorder* →*quasidynamic disorder*→*long-range order*

The physical picture for a slightly doped martensitic system is shown in Figs. 4(b1), 4(b2), 4(b3), and 4(b4). It is important to note that the defects pairs or aggregates create randomly distributed local stresses (expressed by "↔") as shown in Fig. 4(b1), which favor a random distribution of local strain variants. At $T>T_{nd}$ thermal fluctuation is strong and can overcome the defect-induced local stress; hence the system still stays in a dynamically disordered state (i.e., a normal parent phase) in despite of the random stresses. Upon cooling to $T<T_{nd}$, thermal fluctuation becomes weaker and cannot overcome some of the defect-induced local stresses. As a result, a random distribution of static local stresses appears and this results in a random distribution of a small amount of quasistatic local strain domains or nanodomains with the remaining part of the parent phase still flipping dynamically, as shown in Figs. 4(b2) and 4(b3). This quasidynamically disordered strain state below T_{nd} corresponds to the experimentally observed precursor state shown in Fig. 3.

Very interestingly, physically similar quasidynamically disordered state also exists in defect-doped ferroelectric system above the Curie temperature. The onset temperature (from the high-temperature side) of such a state in ferroelectric system is known as the Burns temperature, which signifies the onset of static nanopolar regions in the otherwise ideal paraelectric phase.[39]

As the temperature further decreases to $T<M_s$, the quasidynamically disordered strains undergo a long-range strain ordering, i.e., the formation of martensite, as a consequence of the thermodynamic instability of the parent phase. Thus, the martensitic state of the slightly doped system also shows a normal martensitic transition with multidomain configuration as depicted in Fig. 4(b4), but the domain size is smaller than that in the defect-free system [Fig. 4(a3)]. This is caused by the retardation of the pre-existing quasistatic nanodomains to the domain-growth process.

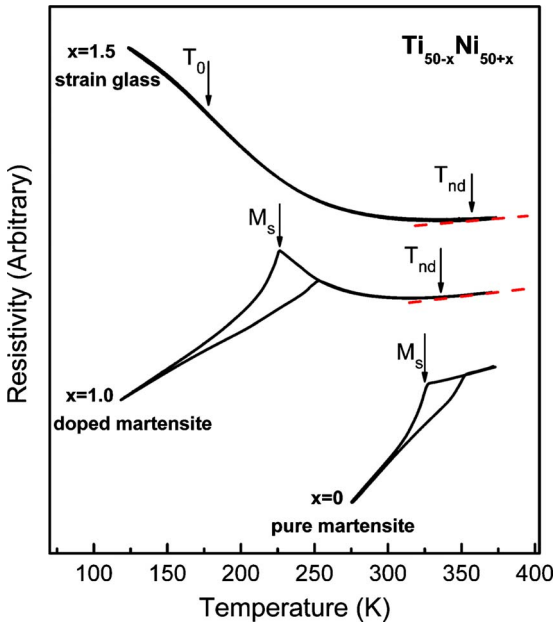

FIG. 6. (Color online) Electrical-resistivity vs temperature curves of $Ti_{50-x}Ni_{50+x}$ for three defect doping levels: undoped ($x=0$), slightly doped ($x=1$), and heavily doped (=strain glass) ($x=1.5$).

3. *High-defect concentration* ($x>x_c$)*: Dynamic disorder* →*quasidynamic disorder*→*frozen disorder*

The physical picture for the martensitic transition in heavily doped martensitic system is shown in Figs. 4(c1), 4(c2), 4(c3), and 4(c4). Similar with the case of the slightly doped system, at $T>T_{nd}$ high temperature, the system is in a dynamically disordered strain state due to the high thermal fluctuation k_BT. At $T<T_{nd}$ the system also changes to the quasidynamically disordered strain state, which is shown from Figs. 4(c1) to 4(c3). However, being different from that of slightly doped system, the high-defect concentration significantly lowers the stability of martensite so that it cannot be formed even at 0 K. On the other hand, with cooling to T_0, thermal energy k_BT becomes lower than the average energy barrier for flipping local domains so that the domain flipping essentially stopped and hence the system is frozen. This process represents a glass transition from a quasidynamically disordered strain state to a frozen disordered strain state, i.e., frozen strain glass [Fig. 4(c4)].

From the above, we can see that excess Ni (as point defects) plays two important roles to form strain glass: (1) reducing the thermodynamic stability of martensite so as to make long-range strain order difficult, as seen from the drastic lowering of M_s with increasing Ni content, (2) forming a random distribution of local stresses/strains. From this we can predict that any ferroelastic/martensitic system with a dopant creating a similar dual effect will result in a strain glass state at high-doping level. Our recent work on Ti-Ni-X (X=Co, Cr, and Mn) and Ti-Pd-Cr ternary system has revealed similar strain glass and similar phase diagram in these system,[18,19] being in agreement with this view.

B. Origin of the decrease and vanishing of transition entropy in $Ti_{50-x}Ni_{50+x}$ with increasing excess Ni

A long-standing puzzle about the martensitic transition of $Ti_{50-x}Ni_{50+x}$ system is the drastic decrease in the transition latent heat or entropy as a function of defect content x, and the entropy eventually vanishes at $x \geq 1.5$, as shown in Fig. 5. As transition entropy reflects the jump in order parameter (lattice strain) at M_s, there seems no reason why such a jump must decrease with increasing defect concentration and must vanish at high-defect concentration. In the following we show that this long-standing puzzle can be well explained by the microscopic picture in Fig. 4.

The transition entropy is proportional to the change in strain order between the parent phase and martensite phase at transition temperature.[40] For a pure $Ti_{50-x}Ni_{50+x}$ ($x=0$) martensitic system, the transition is between a fully strain-disordered parent phase [Fig. 4(a2)] and a fully long-range strain-ordered martensite [Fig. 4(a3)]; thus the transition entropy $\Delta S_{x=0}$ is the largest. For slightly doped alloys ($x<x_c$), the transition is between a partially ordered (locally ordered) parent phase [Fig. 4(b3)] and an imperfectly long-range strain-ordered martensite [Fig. 4(b4)]; thus the difference becomes less. This results in a decrease in transition entropy or latent heat with increasing doping level.

At high-defect content ($x>x_c$), the unfrozen strain glass state with quasidynamically disordered strain [Fig. 4(c3)] cannot form long-range strain ordering but instead gradually freezes into a frozen strain glass state with static disordered strain [Fig. 4(c4)]. Since there is no obvious change in the degree of strain order during strain glass transition, the transition entropy or latent heat becomes negligible in the strain glass composition regime ($x>x_c$).

C. Origin of the defect-induced negative temperature coefficient in electrical resistivity of Ni-rich $Ti_{50-x}Ni_{50+x}$

Many previous studies have found that excess Ni can induce an abnormal increase in electrical resistivity in $Ti_{50-x}Ni_{50+x}$ alloy,[12,14] the so-called negative temperature coefficient of electrical resistivity. Such an effect has remained a puzzle for a long time. To show this effect clearly, the electrical-resistivity curves of $Ti_{50-x}Ni_{50+x}$ with three typical defect compositions $x=0$, 1, and 1.5 are compared in Fig. 6. The electrical resistivity of defect-free $Ti_{50}Ni_{50}$ decreases linearly above its M_s, exhibiting a normal metallic behavior. The electric resistivity of $x=1$ alloy decreases linearly on cooling in high-temperature regime, which is the same metallic behavior as that of parent phase for pure $Ti_{50}Ni_{50}$. However, it gradually deviates from the linear behavior and then followed by a gradual rise with further cooling, until a sudden drop occurring at M_s. For a strain glass composition ($x=1.5$), the abnormal increase in electrical resistivity persists down to 0 K. In the following, we shall show that this defect-induced negative temperature coefficient in electrical resistivity can be explained by the microscopic picture shown in Fig. 4.

The abnormal electrical-resistivity behavior of $x=1$ can be explained by the evolution of the microstructure of a slightly doped martensitic system shown from Figs. 4(b1) to 4(b4). At $T>T_{nd}$ the system is in a dynamically disordered parent state [Fig. 4(b1)], being the same as the pure martensitic system [Fig. 4(a1)]. Thus the electrical resistivity of $x=1$ shows a normal metallic behavior (decreases on cooling) at $T>T_{nd}$. At $T<T_{nd}$ [Figs. 4(b2) and 4(b3)], static nanosized strain domains appear and increase with decreasing temperature. As these nanodomains in Ni-rich $Ti_{50-x}Ni_{50+x}$ alloys possess R-like structure,[4,15,41] and the R phase has a higher specific electrical resistivity compared with that of the B2 parent phase,[42] the formation of R-like nanodomains and the increase in volume fraction at $T<T_{nd}$ cause the deviation from linearity and the gradual increase in electrical resistivity. Thus, the onset temperature T_{nd} for the appearance of R-like nanodomains can be defined as the temperature at which the electrical resistivity deviates from linearity. At $T<M_s$, the electrical resistivity goes down sharply because of the formation of B19′ martensite with lower specific resistivity.

For heavily doped strain glass $x=1.5$, a similar explanation holds as for $x=1$, except that the former does not further change into a martensite. As shown from Figs. 4(c1) to 4(c4), the volume fraction of R-like nanodomains increases continuously with lowering temperature for $T<T_{nd}$, even down to 0 K. This first causes a deviation from linearity in resistivity at $T=T_{nd}$ and then a gradual increase with further cooling down to 0 K, for $x=1.5$ alloy does not go to B19′. At the strain glass transition temperature T_0, there is an inflection point in the resistivity vs temperature curve; this can be interpreted by the fact that freezing makes further formation of R nanodomains difficult and thus reduces the increase rate of the resistivity.

VI. CONCLUSIONS

We systematically studied the transition behavior of $Ti_{50-x}Ni_{50+x}$ as a function of excess Ni concentration x, the following conclusions were obtained. (1) A quantitative phase diagram for $Ti_{50-x}Ni_{50+x}$ (with excess Ni, $0 \leq x \leq 2.5$) is established. It includes not only the known B2 parent phase and B19′ martensite but also a premartensitic phase and a strain glass phase.

(2) We suggest that excess Ni (acting as point defect) plays two key roles in this system: (i) it decreases thermodynamic driving force for forming martensite; (ii) it creates random local stresses that favor local strain ordering. By considering the twofold role of point defects, a general microscopic picture is proposed; it well explains the defect-induced crossover from martensite to strain glass and the formation of precursor nanostructure below T_{nd}.

(3) The gradual decrease and eventual vanishing of transition entropy with increasing excess Ni content are caused by the increase in the local strain order (i.e., precursor nanostructure) in the parent phase and the decrease in the strain order in martensite. In strain glass regime, there is essentially no difference between the high-temperature state and low-temperature state; thus the transition entropy vanishes.

(4) The anomalous negative temperature coefficient of electrical resistivity in Ni-rich Ti-Ni alloys is caused by the appearance of static R-like nanodomains at $T<T_{nd}$ in defect-containing compositions.

ACKNOWLEDGMENTS

The authors gratefully acknowledge the support of National Natural Science Foundation of China (Grants No. 50720145101 and No. 50771079), National Basic Research Program of China (Grant No. 2010CB631003), as well as NCET and 111 project of China.

*Author to whom correspondence should be addressed; ren.xiaobing@nims.go.jp

[1] K. Otsuka and C. M. Wayman, *Shape Memory Materials* (Cambridge University Press, Cambridge, 1998).
[2] K. Otsuka and X. Ren, Prog. Mater. Sci. **50**, 511 (2005).
[3] W. Tang, Metall. Mater. Trans. A **28**, 537 (1997).
[4] V. N. Grishkov, S. F. Dubinin, A. I. Lotkov, V. D. Parkhomenko, V. G. Pushin, and S. G. Teploukhov, Phys. Met. Metallogr. **99**, 435 (2005).
[5] C. Somsen, E. F. Wassermann, J. Kästner, and D. Schryvers, J. Phys. IV **112**, 777 (2003).
[6] S. Semenovskaya and A. G. Khachaturyan, Acta Mater. **45**, 4367 (1997).
[7] S. Kartha, J. A. Krumhansl, J. P. Sethna, and L. K. Wickham, Phys. Rev. B **52**, 803 (1995).
[8] Y. Murakami, H. Shibuya, and D. Shindo, J. Microsc. **203**, 22 (2001).
[9] S. M. Shapiro, J. Z. Larese, Y. Noda, S. C. Moss, and L. E. Tanner, Phys. Rev. Lett. **57**, 3199 (1986).
[10] D. Schryvers and L. E. Tanner, Ultramicroscopy **32**, 241 (1990).
[11] A. Saxena, T. Castán, A. Planes, M. Porta, Y. Kishi, T. A. Lograsso, D. Viehland, M. Wuttig, and M. De Graef, Phys. Rev. Lett. **92**, 197203 (2004).
[12] I. Yoshida, T. Ono, and M. Asai, J. Alloys Compd. **310**, 339 (2000).
[13] S. Miyazaki and K. Otsuka, Metall. Trans. A **17**, 53 (1986).
[14] T. Fukuda, T. Kakeshita, T. Saburi, K. Kindo, T. Takeuchi, M. Honda, and Y. Miyako, Physica B **237-238**, 609 (1997).
[15] S. Sarkar, X. Ren, and K. Otsuka, Phys. Rev. Lett. **95**, 205702 (2005).
[16] K. Binder and W. Kob, *Glassy Materials and Disordered Solids* (World Scientific, Singapore, 2005).
[17] C. A. Angell, Science **267**, 1924 (1995).
[18] Y. Zhou (unpublished).
[19] Y. Zhou, D. Xue, X. Ding, K. Otsuka, J. Sun, and X. Ren, Appl. Phys. Lett. **95**, 151906 (2009).
[20] X. Ren, Y. Wang, K. Otsuka, P. Lloveras, T. Castán, M. Porta, A. Planes, and A. Saxena, MRS Bull. **34**, 838 (2009).
[21] Y. Wang, X. Ren, and K. Otsuka, Mater. Sci. Forum **583**, 67 (2008).
[22] Y. Wang, X. Ren, K. Otsuka, and A. Saxena, Acta Mater. **56**, 2885 (2008).
[23] J. A. Mydosh, *Spin Glasses* (Taylor & Francis, London, 1993).
[24] Y. Wang, X. Ren, K. Otsuka, and A. Saxena, Phys. Rev. B **76**, 132201 (2007).
[25] Y. Wang, X. Ren, and K. Otsuka, Phys. Rev. Lett. **97**, 225703 (2006).
[26] D. Viehland, S. J. Jang, L. E. Cross, and M. Wuttig, J. Appl. Phys. **68**, 2916 (1990).
[27] D. Viehland, S. J. Jang, L. E. Cross, and M. Wuttig, Philos. Mag. A **64**, 835 (1991).
[28] D. Viehland, J. F. Li, S. J. Jang, L. E. Cross, and M. Wuttig, Phys. Rev. B **46**, 8013 (1992).
[29] X. Ren, Y. Wang, Y. Zhou, Z. Zhang, D. Wang, G. Fan, K. Otsuka, T. Suzuki, Y. Ji, J. Zhang, Y. Tian, S. Hou, and X. Ding, Philos. Mag. **90**, 141 (2010).
[30] T. Yamamoto, M. S. Choi, S. Majima, T. Fukuda, T. Kakeshita, E. Taguchi, and H. Mori, Philos. Mag. **88**, 1027 (2008).
[31] G. Burns, Phys. Rev. B **13**, 215 (1976).
[32] G. Burns and F. H. Dacol, Phys. Rev. B **28**, 2527 (1983).
[33] J. R. Morris and R. J. Gooding, Phys. Rev. Lett. **65**, 1769 (1990).
[34] M. F. Collins, V. J. Minkiewicz, R. Nathans, L. Passell, and G. Shirane, Phys. Rev. **179**, 417 (1969).
[35] R. Z. Tai, K. Namikawa, A. Sawada, M. Kishimoto, M. Tanaka, P. Lu, K. Nagashima, H. Maruyama, and M. Ando, Phys. Rev. Lett. **93**, 087601 (2004).
[36] Ll. Mañosa, M. Jurado, A. Planes, J. Zarestky, T. Lograsso, and C. Stassis, Phys. Rev. B **49**, 9969 (1994).
[37] A. G. Khachaturyan, *Theory of Structural Transformation in Solids* (Wiley, New York, 1983).
[38] E. K. H. Salje, *Phase Transformation in Ferroelastic and Co-Elastic Crystals* (Cambridge University Press, Cambridge, 1993).
[39] Z. Xu, M. C. Kim, J. F. Li, and D. Viehland, Philos. Mag. A **74**, 395 (1996).
[40] G. Careri, *Order and Disorder in Matter* (Addison-Wesley, Reading, MA, 1984).
[41] D. Shindo, Y. Murakami, and T. Ohba, MRS Bull. **27**, 121 (2002).
[42] S. Miyazaki and K. Otsuka, Philos. Mag. A **50**, 393 (1984).